TIMELESS mutation alters phase responsiveness and causes advanced sleep phase

Philip Kurien[a,1], Pei-Ken Hsu[b,1,2], Jacy Leon[a], David Wu[b], Thomas McMahon[b], Guangsen Shi[b], Ying Xu[c], Anna Lipzen[d,e], Len A. Pennacchio[d,e], Christopher R. Jones[f], Ying-Hui Fu[b,g,h,3], and Louis J. Ptáček[b,g,h,3]

[a]Department of Anesthesiology, University of California, San Francisco, CA 94143; [b]Department of Neurology, University of California, San Francisco, CA 94143; [c]Center for Systems Biology, Soochow University, Suzhou 215000, China; [d]Genomics Division, Lawrence Berkeley National Laboratory, Berkeley, CA 94720; [e]Department of Energy Joint Genome Institute, Walnut Creek, CA 94598; [f]Department of Neurology, University of Utah, Salt Lake City, UT 84132; [g]Weill Neuroscience Institute, University of California, San Francisco, CA 94143; and [h]Kavli Institute for Fundamental Neuroscience, University of California, San Francisco, CA 94143

Many components of the circadian molecular clock are conserved from flies to mammals; however, the role of mammalian Timeless remains ambiguous. Here, we report a mutation in the human *TIMELESS* (h*TIM*) gene that causes familial advanced sleep phase (FASP). *Tim* CRISPR mutant mice exhibit FASP with altered photic entrainment but normal circadian period. We demonstrate that the mutation prevents TIM accumulation in the nucleus and has altered affinity for CRY2, leading to destabilization of PER/CRY complex and a shortened period in nonmature mouse embryonic fibroblasts (MEFs). We conclude that TIM, when excluded from the nucleus, can destabilize the negative regulators of the circadian clock, alter light entrainment, and cause FASP.

TIMELESS | human genetics | mammalian circadian clock regulation | familial advanced sleep phase

The circadian clock governs the timing of many body functions (1), including the onset and offset of sleep, that oscillate with a ~24-h period (2–5). The mammalian core clock is composed of the positive transcription activators, BMAL1 and CLOCK, and the key negative regulators, PERs and CRYs (3–5). In recent years, studies of human circadian phenotypes have contributed significantly to a better understanding of the molecular clock. Familial advanced sleep phase (FASP) is an inherited condition where affected subjects wake and sleep early (6). We previously showed mutations in the genes (*PER2, CRY2, PER3*) for negative regulators of the clock that cause the FASP phenotype (7–9). A common feature of these identified mutations is the instability of PER and CRY, causing derepression of BMAL1/CLOCK. This leads to a shortened circadian period and advanced sleep phase. While we have demonstrated that the shortened period is sufficient to cause FASP (7, 8), a mutation that alters entrainment could potentially produce the FASP phenotype with preserved period (10).

Although studies have shown the importance of key conserved components of the circadian clock across species (4), much remains unknown of the role for mammalian homologs of *Drosophila Timeless* (*Tim*). Tim is a core component of the *Drosophila* (d) clock, and it functions as the light-sensitive partner of dPer to provide the negative regulation necessary for generating rhythmicity and photoentrainment in flies (11–13). Based on phylogenetic analysis, mammalian [both mouse (m) and human (h)] *Tim* has higher sequence homology to *Drosophila Timeless2* (*Tim2*), which was shown to participate in DNA metabolism, maintenance of chromosomal integrity, and light entrainment of the adult clock (14). Homozygosity for m*Tim* knockout is embryonic lethal (at the preimplantation stage), and analysis of viable heterozygous m*Tim* mutant mice showed no change in circadian period (15). Previous studies have shown that m*Tim* levels in the suprachiasmatic nucleus (SCN) oscillate over circadian time with a peak of expression at the day–night transition, similar to that of m*Per2* (16). Conditional knockdown of *Tim* disrupted the rhythmic neuronal firing in ex vivo rat SCN slices, affected the expression of other core clock proteins, and altered phase responsiveness in tissues (17). In addition, func-

tional analysis of truncated TIM revealed the role of the N-terminal portion in binding to partners like CRY and the C-terminal domain for nuclear translocation (18). These data clearly implicate a role for TIM in mammalian circadian regulation; however, a precise functional mechanism for its contribution remains incomplete.

We report a mutation in the human *TIMELESS* gene that is responsible for the FASP phenotype in a family. CRISPR-generated mutant mice recapitulate the advanced sleep phase phenotype with normal period and altered light entrainment properties. Moreover, shortened period was found in CRISPR-generated cells and mouse embryonic fibroblasts (MEFs). The mutant protein has lower stability, exclusive cytoplasmic localization, reduced affinity for CRY2, and exerts weakened repression on CLOCK-BMAL1 induced expression. Importantly, we found that wild-type (WT) TIM can destabilize the PER2–CRY2 complex and the mutation enhances this function of TIM. These results indicate that mammalian TIM plays a role in regulating circadian clock by fine-tuning levels of the PER2–CRY2 complex.

Results

Identification of a *TIMELESS* Mutation in a Family with FASP. We had identified a family with two FASP individuals and one non-FASP subject (Table 1). The actigraphy recording showed that the

> ### Significance
>
> TIMELESS has a clear role in the regulation of circadian rhythms in *Drosophila*, but its role in mammalian circadian regulation remains unclear. A mutation identified in a small family with advanced sleep phase causes cytoplasmic accumulation of TIMELESS. We confirm that TIMELESS can bind the critical negative regulators of the circadian clock, PER2 and CRY2, and destabilize them when TIMELESS remains in the cytoplasm. The mutant mouse model has a phase advance of sleep–wake behavior and altered sensitivity to light pulses, but normal period length. These data demonstrate that TIMELESS may play a role in regulating minor phase changes and therefore contribute to the maintenance of circadian rhythmicity in mammals.

non-FASP subject had an apparent discordance between sleep/wake times relative to activity onset and offset times, which is likely due to movement captured by actigraphy after the onset of sleep and before wake onset. A nonsense mutation in h*TIM* (see nomenclature in *Materials and Methods*) was identified in this FASP family by two independent screening approaches. We first employed candidate gene screening of 25 circadian clock-relevant genes (7). An unbiased whole-exome sequencing was subsequently applied to confirm the identified mutation (Fig. 1*A*). This mutation changes an arginine to a stop codon at amino acid position 1081 (*TIMELESS R1081X, TIM R1081X*). The mutation causes the loss of 128 aa at the C-terminal end of the conserved TIMELESS_C domain (Fig. 1*B*; for complete regional alignment, see *SI Appendix,* Fig. S1*D*) (19–21), which contains the fourth and last putative nuclear localization signal (NLS4) conserved among mammalian species (18). The *TIM R1081X* mutation and the FASP phenotype cosegregate in this family (Fig. 1*A*) (6, 22), although the family is too small to prove this locus is linked. Thus, additional in vitro and in vivo experiments were required to prove causation. This mutation has not been reported in the SNP databases.

Measuring Circadian Period of *Tim R1078X* Mice and Cells. To further examine the circadian phenotype of the human *TIM R1081X* mutation in vivo, we generated CRISPR-edited mice (*Tim R1078X*) harboring the causative mutation at the conserved codon position (R1078 in mouse) (*SI Appendix,* Fig. S1 *A–C*). *Tim R1078X* (*RX*/+) heterozygous and *WT* (+/+) littermate mice were subjected to circadian behavior testing, first entrained under conditions of 12-h light and 12-h darkness (LD 12:12) before being released into constant darkness (DD) to determine the endogenous circadian period. The free-running period of *RX*/+ mice (23.60 ± 0.043 h) was not significantly different from that of +/+ controls (23.71 ± 0.022 h; Fig. 2 *A* and *B*) by line fitting analysis.

To test whether the heterozygous *TIM R1081X* mutation at the endogenous locus is sufficient to cause shortened period in vitro, a U2OS cell line with a heterozygous *TIM R1081X* mutation was generated by CRISPR-mediated genome editing (Fig. 2*C*). Out of 128 edited clones, a single clone (no. 37) with heterozygous *R1081X*/+ genotype (green dots; genotyping done in duplicates; Fig. 2*D*) was identified and verified by Sanger sequencing (Fig. 2*E*). The heterozygous *R1081X*/+ U2OS cells showed ~29-min shortening of period compared with +/+ cells (23.29 vs. 23.78 h; Fig. 2*F*).

Circadian period was further assessed in peripheral tissues of *RX*/+ and +/+ mice that had been crossed to m*Per2^Luc* knockin mice (23). Similar to what was observed for the running period of mice, liver and lung ex vivo cells showed no period change (*SI Appendix,* Fig. S2*A*). Although *Tim* expression had previously been reported to be low in nonproliferative tissues (18), we further confirmed TIM expression levels in proliferative and nonproliferative tissues and in MEFs (*SI Appendix,* Fig. S2 *D–F*). We next examined periodicity using MEFs from these mice and observed a modest yet significant reduction in period in *RX*/+ MEFs compared with +/+ MEFs (24.0 vs. 24.36 h; *SI Appendix,* Fig. S2*B*). Moreover, expression of TIM R1081X in HEK293T cells shortened the period by ~37 min compared with HEK293T cells

expressing TIM WT (25.92 vs. 26.54 h; *SI Appendix,* Fig. S2*C*), similar to the shortened period phenotype observed in MEFs.

h*TIM R1081X*/m*Tim R1078X* Mutation Alters Light Entrainment. We next assessed light entrainment in the mutant mice. In LD 12:12 (lights on 0600–1800), no change in the activity onset and offset was seen (Fig. 2*A*). Light masking is a strong confounding factor when examining locomotor behavior to assess phase in LD 12:12 (24, 25). Therefore, we entrained mice to a skeleton photoperiod to minimize the masking effect of light with 15-min light arms from clock times 06:00 to 06:15 and again from clock times 17:45 to 18:00, with darkness at all other times. Under these conditions, activity onset was significantly advanced in heterozygous *RX*/+ mice compared with +/+ mice (−40.32 ± 12.53 min vs. 9.545 ± 6.756 min) (Fig. 3 *A–C*). Activity offset was more heterogenous in the skeleton photoperiod without a significant difference of offset of activity in mutant animals (−18.13 ± 15.37 min vs. 14.73 ± 7.397 min; Fig. 3 *A–C*). Since rest and activity behavior quantification is a surrogate for sleep/wake states and is influenced by the effect of light masking, we subjected mice to electroencephalography (EEG) assessment in LD 12:12 to objectively score sleep/wake epochs. Phase advance of wakefulness and sleep at the transition from light to dark and from dark to light was ~30 min (Fig. 3*D*). Under LD 12:12, overall sleep duration, sleep bout length and number, and total nonrapid eye movement (NREM) and REM sleep percentages were preserved (*SI Appendix,* Fig. S3 *A* and *B*), indicating that the advanced phase is gated by circadian parameters and does not affect sleep architecture.

The strength of entrainment was examined using 30-min light pulses at Zeitgeber time (ZT) 14 and ZT 22 and by assessing the magnitude of phase shift in either condition compared with the activity onset in the absence of a light pulse (baseline). Heterozygous *RX*/+ mice exhibited a significantly increased phase advance after initial release into DD compared with +/+ mice (30.22 ± 5.125 min vs. 4.886 ± 4.324 min; Fig. 3*E, Upper* panels and leftmost graph). Heterozygous *RX*/+ mice exhibited a significantly longer phase delay with a light pulse at ZT 14 compared with +/+ controls (−77.11 ± 12.20 min vs. −21.41 ± 13.41 min; Fig. 3*E, Middle* panels and middle graph). The ZT 22 light pulse elicited a diminished phase advance from *RX*/+ mice (−3.686 ± 5.916 min vs. 41.20 ± 10.15 min; Fig. 3*E, Lower* panels and rightmost graph). These data indicate that the *TIM R1081X* mutation changes sensitivity to entraining stimuli, a finding that is consistent with previous studies of timed *Tim* knockdown in ex vivo rat SCN slices (17).

TIM R1081X Is Less Stable and Localized to the Cytoplasm, and TIM R1081X-Expressing Cells Have Reduced Repressor Activity. We next examined the molecular alterations underlying the observed changes in period and entrainment. Since inhibition of CLOCK-BMAL1 transactivation by hTIM had been shown previously (20), we tested the repressor activity of TIM R1081X. TIM WT expression inhibited the CLOCK-BMAL1−mediated luciferase expression in a dose-dependent manner, resulting in a more than 80% decrease in CLOCK-BMAL1−induced luciferase activity at the highest dosage (9.92 vs. 1.84 normalized luciferase activity,

Table 1. Clinical variables of human subjects in a FASP family

Subject	Age	Status	Activity offset	Sleep onset	Activity onset	Wake onset	H-O score
101305	80	C	21.84	22.40	5.06	4.92	73
35357*	54	C	21.77	22.36	5.65	5.25	70
101316	55	NC	22.61	22.25	7.15	7.40	57

C, mutation carrier; NC, mutation noncarrier; H-O, Horne–Ostberg.
*Proband.

A K5602

RX/+
101305

RX/+   +/+
35357   101316

C --> T
R1081X

■ Status = Affected
□ Status = Unaffected

B

Human   24   TIMELESS   284   728   TIMELESS_C   1208

Mouse   24   TIMELESS   284   722   TIMELESS_C   1196

                                                        *
Consensus   A-PLVPLTEENEEAAMEN-QFQ-LLRKLG-RPP-SGQETFWRIPAKL
TIM [Homo sapiens]   AVPLVPLTEENEEAMENEQFQQLLRKLGVRPPASGQETFWRIPAKL   1086
TIM [Pan troglodytes]   AVPLVPLTEENEEAMENEQFQQLLRKLGVRPPASGQETFWRIPAKL   1087
Tim [Mus musculus]   AIPLVPLTEENEEAMENEQFQHLLRKLGIRPPSSGQETFWRIPAKL   1083
Tim [Rattus norvegicus]   AIPLVPLTEENEEAMENKQFQHLLRKLGIRAPCSGQETFWRIPAKL   1085
Tim [Drosophila melanogaster] SIPVVQWNNEQSTTMLYQPFVLLLHKLGIQLPADAGSIFARIPDYW   1096
Timeout [Droso... melanogaster] GVPLLPLMENQKNAMEDGDFQKVLVALGMQPPISGMEAYWRIPIYL   1100

Consensus   S-TQLRR-AASL-------------S--E---E-E----------
TIM [Homo sapiens]   SPTQLRRAAASL-------------SQPEEEQKLQ-----------   1132
TIM [Pan troglodytes]   SPTQLRRVAASL-------------SQPEEEQKLQ-----------   1133
Tim [Mus musculus]   SSTQLRRVAASL-------------SQQENEEERE-----------   1129
Tim [Rattus norvegicus]   SSTQLRRVAASL-------------SERENKEEREE----------   1131
Tim [Drosophila melanogaster] TPETMYGLAKKL-------GPLDKLNLKFDASELEDATASSPSRYH   1140
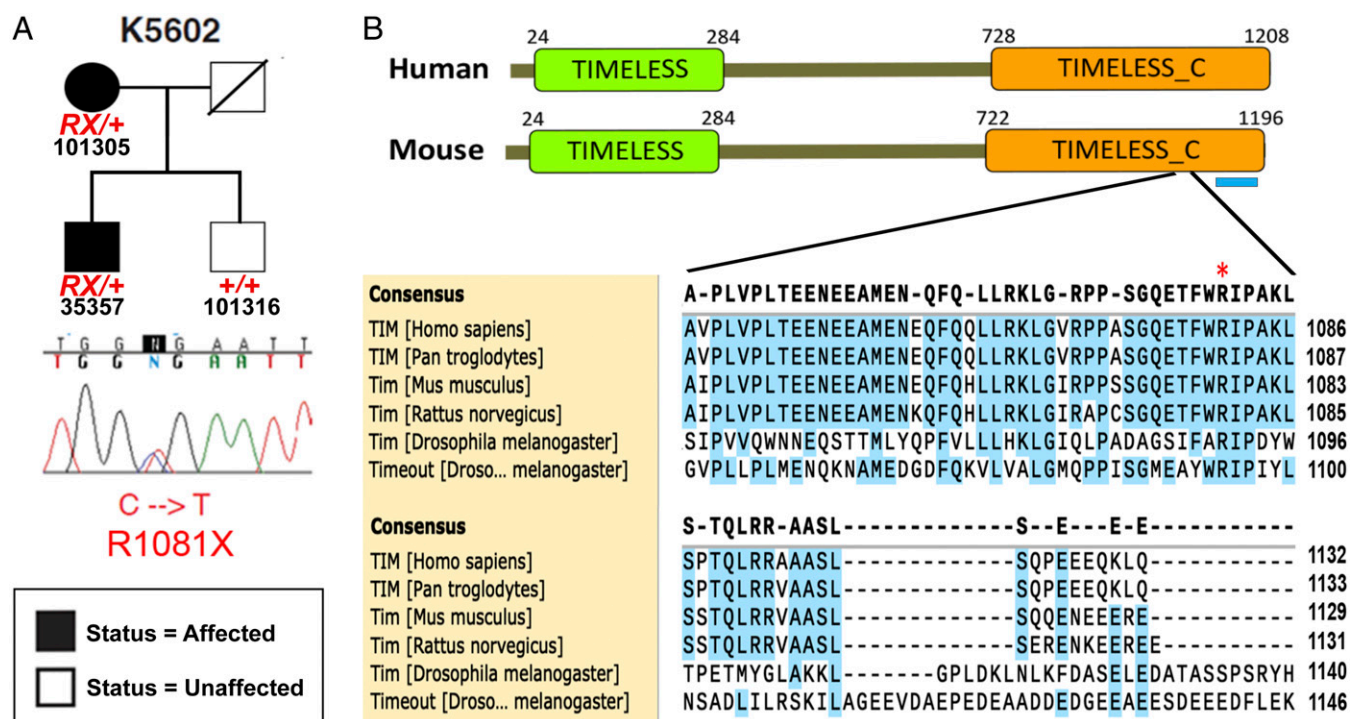Timeout [Droso... melanogaster] NSADLILRSKILAGEEVDAEPEDEAADDEDGEEAEESDEEEDFLEK   1146

Fig. 1. *TIMELESS R1081X* mutation found in a FASP family. (*A*) In kindred 5602, a *TIMELESS R1081X* nonsense mutation cosegregates with FASP. Filled and open shapes represent affected and unaffected individuals, respectively. Circles and squares represent women and men, respectively. Individuals with the *R1081X* mutation are heterozygous. (*B*) The *TIMELESS R1081X* mutation is located in the conserved TIMELESS_C domain. On the *Lower Right*, the amino acid alignment around the *R1081X* mutation (marked by a red asterisk) is shown. A blue rectangle (below the diagram) marks the last putative nuclear localization signal in the TIMELESS protein (NLS4). The mutation causes a truncated protein lacking NLS4.

with or without TIM WT, respectively; Fig. 4*A*). Overall repressor activity for CLOCK-BMAL1−mediated expression is weaker in TIM R1081X-expressing cells vs. TIM WT-expressing cells across different dosages with a significant genotype effect ($P < 0.01$) and dosage effect ($P < 0.001$) without a genotype–dosage interaction.

Mutations that destabilize transcriptional repressors in the circadian transcription–translation feedback loop can speed up the circadian clock and shift sleep phase (7, 26, 27). We therefore examined the protein stability of TIM WT and TIM R1081X by assessing the decline in protein levels after cycloheximide (CHX) treatment and found that TIM R1081X is less stable than TIM WT (Fig. 4*B*), with a significant genotype effect ($P < 0.01$), and time effect ($P < 0.001$), but no genotype–time interaction.

TIM R1081X leads to a truncated protein lacking a putative nuclear localization signal (NLS4, see Fig. 1*B* and *SI Appendix,* Fig. S1*D*), which has been shown to be necessary and sufficient for nuclear localization (18). Indeed, in contrast to TIM WT (predominantly localized in the nucleus), TIM R1081X is mostly cytoplasmic, as shown by both immunocytochemistry (66.9% vs. 23.7% nuclear TIM signal, WT vs. R1081X; Fig. 4*C*) and Western blotting (94% vs. 34% nuclear TIM signal, WT vs. R1081X; Fig. 4*D*). These findings indicate that the last 128 aa (including the NLS4) of mammalian TIMELESS is critical for proper nuclear translocation of TIM.

To determine whether the loss of NLS4 contributes to the molecular deficit underlying the TIM-R1081X phenotypes, we generated TIM without NLS4 (TIM-ΔNLS4). We found that TIM-ΔNLS4 is restricted to cytoplasm, and the period of TIM-ΔNLS4–expressing cells is shortened compared with that of the TIM WT-expressing cells (*SI Appendix,* Fig. S4 *A* and *B*). Taken together, our results suggest that the *TIM-R1081X* mutation leads to FASP partly due to the loss of NLS4.

TIM-R1081X Has Weakened Interaction with CRY2 and Leads to Destabilization of CRY1/2 and PER1/2. Since TIM was shown to bind CRY proteins (18, 28), we examined whether the *TIM R1081X* mutation affects interactions between TIM and CRY2. Upon immunoprecipitation of CRY2, the abundance of coimmunoprecipitated TIM R1081X was only 2.8% of bound TIM WT (Fig. 5*A*). Consistently, the amount of CRY2 coimmunoprecipitated with TIM R1081X was 48.7% less than the amount bound to TIM WT (*SI Appendix,* Fig. S5*A*). These results indicate that the 128-aa C-terminal region of TIMELESS protein is required for stabilizing its interaction with CRY2 protein.

TIM was shown to bind PER2 in the SCN (17) but not in cell culture systems (18). Given the interaction of TIM with CRY2, we sought to reexamine whether PER2 and TIM interact and whether the TIM R1081X mutation alters any putative association with PER2. We found that PER2 coimmunoprecipitated with both WT and R1081X TIM, but unlike CRY2, the interaction was not affected by the mutation (Fig. 5*B* and *SI Appendix,* Fig. S5*B*).

The stability and levels of major repressors of the molecular clock are critical for the regulation of clock speed (7). Because both PER2 and CRY2 can bind to TIM R1081X and TIM WT but with different affinities, we investigated whether the stability of PER2 or CRY2 is altered by the TIM R1081X mutation. HEK 293T cells were transfected with either *TIM R1081X* or *TIM WT* together with either *CRY2:luc* or *PER2:luc,* and the stabilities of PER2 and CRY2 were assayed after CHX treatment. The half-life of both CRY2 and PER2 were significantly reduced in *TIM R1081X*-transfected cells compared with *TIM WT*-transfected or empty vector control cells (*SI Appendix,* Fig. S5*C*). Similarly, the half-life of both CRY1 and PER1 were significantly reduced in *TIM R1081X*-transfected cells compared with *TIM WT*-transfected or control cells (*SI Appendix,* Fig. S5*D*). These results suggest that PER1/2 and CRY1/2 interacts with TIM and
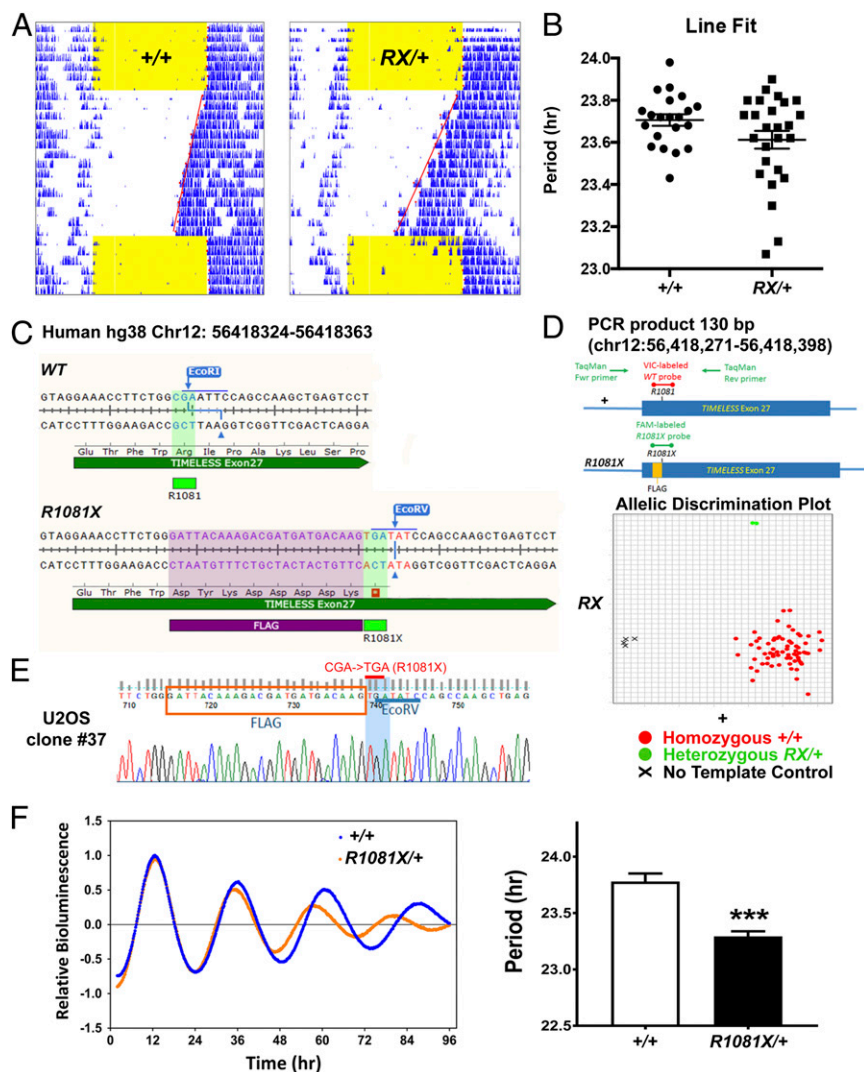
Fig. 2. A heterozygous h*TIM R1081X*/m*Tim R1078X* mutation was generated by genome editing and results in shortened period in cells but not in mice. (*A*) Representative actograms of wheel-running activity for *Tim* +/+ (*Left*) and *RX*/+ (*Right*) mice. Yellow marks the times when the lights were on. Blue marks wheel-running activity. Each row represents a single day. Activity onset was fitted to the red lines using ClockLab analysis software. (*B*) Period for *RX*/+ and +/+ mice was determined by line fitting of activity onset from day 1 to day 14 in DD (constant darkness) ($n = 21$ for +/+, $n = 26$ for *RX*/+), $P > 0.05$ (Student's *t* test). (*C*) *Upper* panel shows the *TIM* exon 27 genomic locus (hg38, Chr12: 56418324–56418363, negative strand orientation) with the R1081 codon marked and highlighted in green. There is an EcoRI site overlapping the R1081 codon. Lower view shows the edited *TIM R1081X* allele in that genomic locus. The mutated nucleotides are in red, and the R1081X codon is marked and highlighted in green. A FLAG sequence was also inserted before the stop codon. The codon next to R1081X was mutated to create an EcoRV site for genotyping. (*D*) The *Upper* panel shows a schematic of TaqMan-based genotyping design with specific fluorescence probes to either + or *R1081X* alleles. The *Lower* panel is the allelic discrimination plot of the genotype screening assays on CRISPR-edited U2OS cell clones. Fluorescence of probes to + and *R1081X* alleles are shown on the x and y axis, respectively. Red and green dots represent homozygous +/+ and heterozygous *R1081X*/+ clones. The genotyping assay was done in duplicate. (*E*) Representative Sanger sequencing trace of TA clones of U2OS clone 37 confirming the *R1081X* allele and the EcoRV site. (*F*) On the *Left* are representative rhythms of *Bmal1-luc* reporter in U2OS-B6 cell lines with +/+ and *R1081X*/+ genotype at endogenous *TIM* genomic locus. Data were detrended, normalized to the peak bioluminescence, and aligned to the first peak. Periods of the bioluminescence rhythm in the *TIM* +/+ and *R1081X*/+ cells are quantified on the *Right*. Results are expressed as mean ± SEM ($n = 8$). ***$P < 0.001$ (Student's *t* test).

that TIM destabilizes these proteins when restricted to cytoplasm. To examine the effect of *TIM R1081X* on the stability of the PER2–CRY2 heterodimer, we cotransfected cells with *TIM WT* or *TIM R1081X* together with *PER2* (or *CRY2*) and *CRY2:luc* (or *PER2:luc*) constructs and assayed the stability of CRY2:luc (or PER2:luc). TIM WT expression results in CRY2 and PER2 having intermediate stability compared with vector control or TIM R1081X (Fig. 5*C*). The destabilizing effect of TIM WT on the PER2-CRY2 complex is dose dependent (Fig. 5*C*, *Right* panels). These results imply a role for TIM WT as a destabilizer of the PER–CRY complex, and this destabilization effect of TIM is enhanced by the *R1081X* mutation.

Discussion

Although the role of mammalian TIMELESS in circadian regulation has been ambiguous, its transcriptional repression activity for CLOCK/BMAL1 and interactions with mPER1/mCRY have previously been demonstrated (18, 22, 29). Here, we report that a mutation in human *TIMELESS R1081X* causes FASP leading to reduced nuclear presence of TIM and reduced stability of PER1/2 and CRY1/2.

With the exception of the *PER2 S662G* FASP phenotype, the other reported mutations found in families with FASP (*CRY2, CK1δ, PER3*) show subtle phenotypes in mouse models (7, 9, 27). This is expected given that carriers of these mutations are
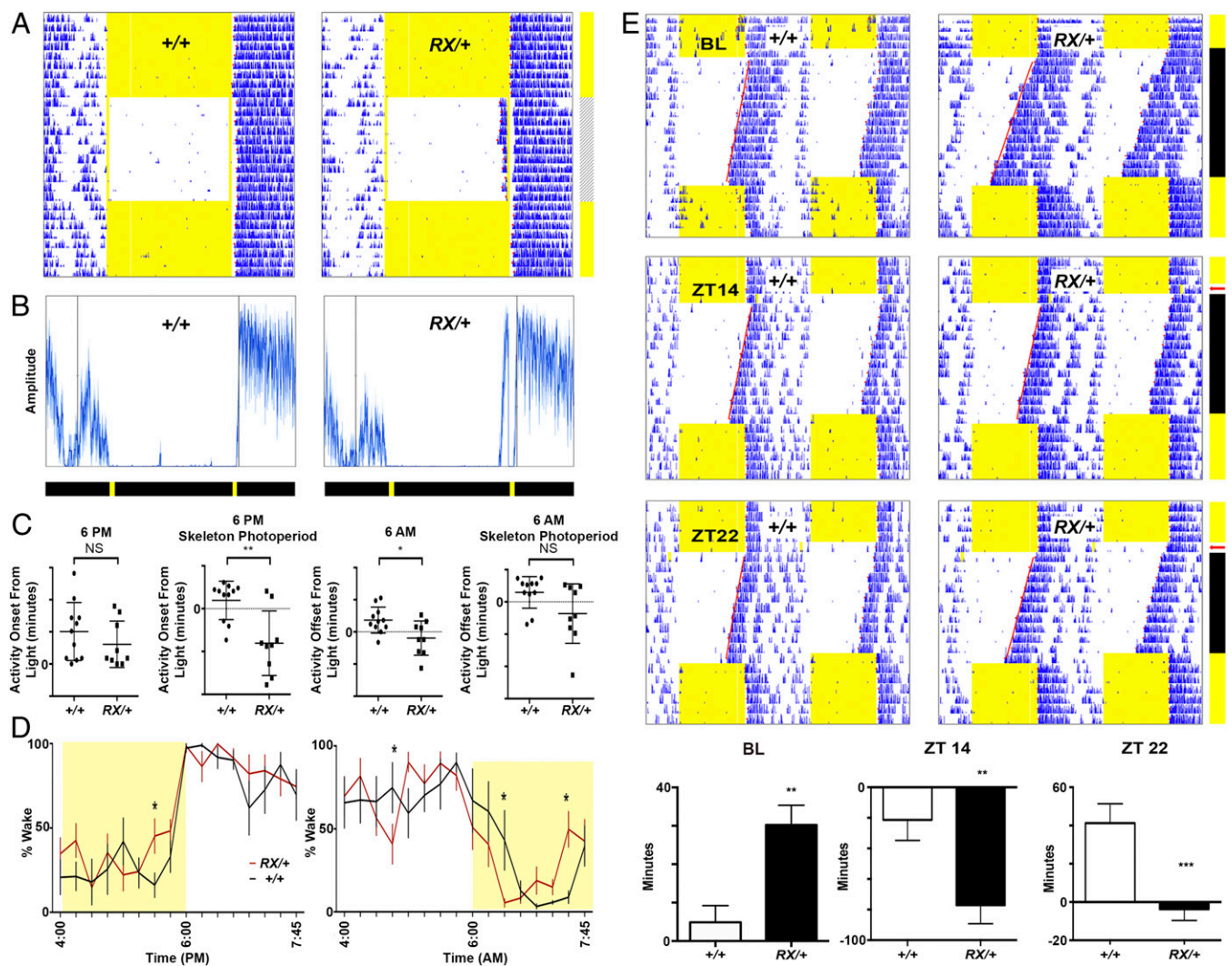
Fig. 3. Heterozygous *TimRX* mutant mice have advanced phase of sleep–wake behavior and altered phase responsiveness to timed light pulses. Representative actograms (*A*) and activity profiles (*B*) of wheel-running activity for +/+ and *RX*/+ mice under skeleton photoperiod with 15-min entraining arms for an 11-d period. Each row represents a single day. The yellow and gray bars in *A* (*Right*) represent LD 12:12 entrainment and skeleton photoperiod paradigms, respectively. The black and yellow bars in *B* (below) represent periods of darkness and light, respectively. The *y* axis represents wheel-running amplitude. (*C*) Activity onset/offset from the onset of the light pulse. "0" represents light onset/offset; each hash mark reflects 10 min in the leftmost panel and 50 min in the three rightmost panels. Results are expressed as mean ± SEM (*n* = 11 for +/+; *n* = 9 for *RX*/+). *$P < 0.05$; **$P < 0.01$; NS, not significant (Student's *t* test). (*D*) Wake percentage from EEG recordings in LD 12:12 at the time of light transition. Time epochs representing the change from lights-on to lights-off (*Left*), and lights-off to lights-on (*Right*) are shown. Each hash mark below represents a 15-min interval. The yellow blocks indicate lights-on. Wake percentage is provided in the *y* axis (*n* = 6 for +/+, *n* = 9 for *RX*/+). *$P < 0.05$ (two-way ANOVA and post hoc multiple comparison with Fisher's test). (*E, Top*) Representative double-plotted actograms showing baseline behavior (BL) in LD 12:12 and in DD, and phase shifts (below) in response to a 30-min light exposure at ZT 14 and ZT 22 indicated by red arrows. Each row represents 2 d. (*E, Bottom*) Average phase shifts by minutes for BL, ZT 14, and ZT 22 (*n* = 15 for +/+; *n* = 20 for *RX*/+). **$P < 0.01$, ***$P < 0.001$ (Student's *t* test).

normal, healthy humans. The *RX*/+ mutant mice have advanced phase of activity onset in conditions where light masking is minimized while activity offset was not advanced in the skeleton photoperiod due to higher variability in offsets. Phase advance of both wake onset and offset was confirmed with EEG analysis under standard lighting conditions (Fig. 3*B*). EEG data also revealed that the overall quantity of sleep was preserved (*SI Appendix*, Fig. S3 *A* and *B*).

Common features of the previously reported circadian mutants include altered period of variable magnitude (22–23.4 h) and changes in entrainment. The *TIM R1081X* mutation is an example of an advanced phase phenotype and altered entrainment without significant change in period compared with WT at the organismal level. We previously posited that the FASP

phenotype can result from either a shortened circadian period or altered entrainment. *TIM R1081X* represents a model in which advanced sleep phase (ASP) is present in the setting of an altered entrainment phenotype, but in the absence of period shortening in vivo. The period shortening and protein instability demonstrated in vitro when TIM is expressed at higher levels in tissues or cells suggests that the phase phenotype could be a function of low TIM expression and the period shortening only happens when TIM is more highly expressed. Forward mutagenesis screens in model organisms have focused primarily on phenotypes of arrhythmicity and altered period. Because our human genetic studies of FASP have focused on a phase phenotype (rather than period), we expected to find mutations affecting period and/or entrainment. The finding of altered entrainment in
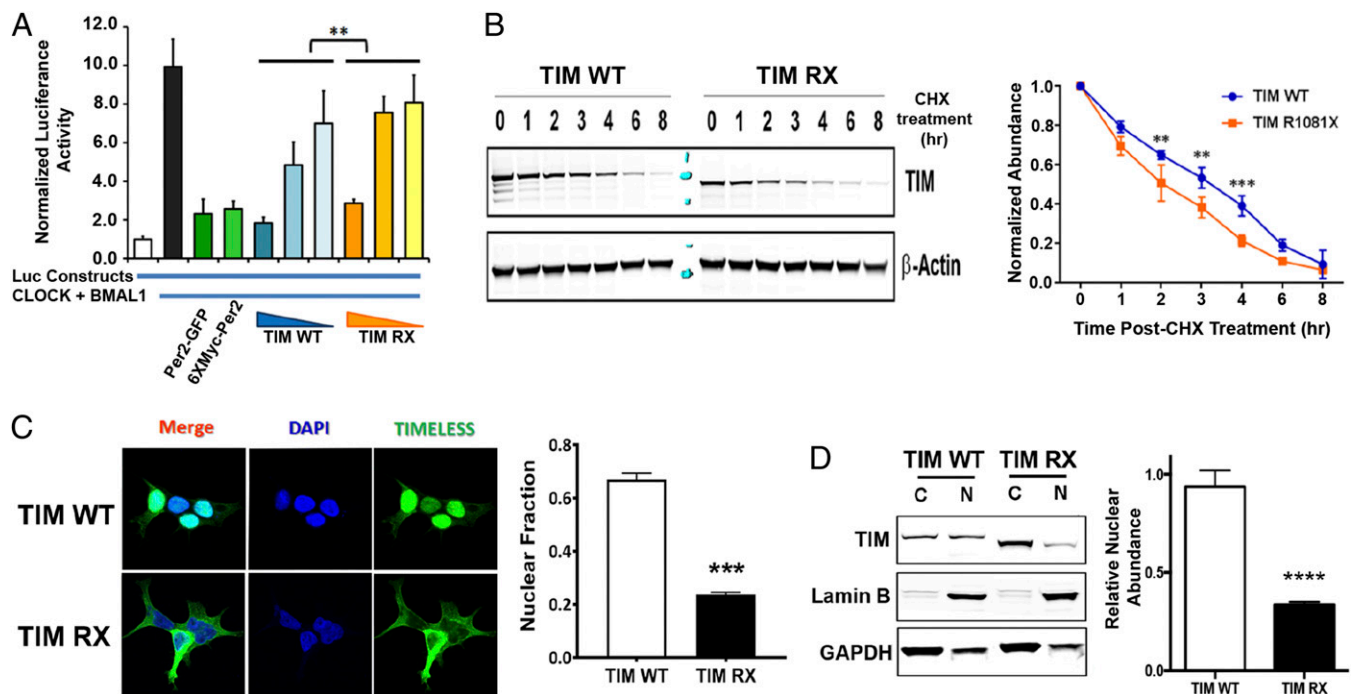
Fig. 4. Altered molecular function of TIM by the R1081X mutation. (*A*) Repressor activity of WT or R1081X TIM on CLOCK-BMAL1–mediated expression was examined with *Per2* promoter-driven luciferase activity in HEK293T cells. Luciferase activity was normalized to activity levels in cells without CLOCK/BMAL1 (white column). PER2 from two different constructs were positive controls for repressor activity. Genotype effect: **$P < 0.01$ (two-way ANOVA). (*B*) Western blot and time course of TIM-WT and TIM-R1081X abundance after cycloheximide (CHX) was supplied to transfected 293T cells. Results are expressed as mean $\pm$ SEM ($n = 3$). Genotype effect: **$P < 0.01$, ***$P < 0.001$ (two-way ANOVA). (*C*) Immunocytochemistry demonstrates the subcellular localization of TIM WT and TIM R1081X in 293T cells 24 h posttransfection. Boundaries of nuclei were determined, and the proportion of TIMELESS signal within the nucleus vs. whole cell (nuclear fraction) was quantified ($n = 20$–25 each group). ***$P < 0.001$ (Student's *t* test). (*D*) Western blot of TIM WT and TIM R1081X protein in enriched nuclear and cytoplasmic fractions. Lamin B and GAPDH were nuclear and cytoplasmic markers, respectively. Relative intensities of TIM were quantified and are shown on the *Right* ($n = 5$). ****$P < 0.0001$ (Student's *t* test).

the absence of period shortening in this *TIM* mutant validates this idea. The difference in the baseline phase after release into DD between *TIM* mutant and WT animals (Fig. 3*E*) may reflect a combination of the derepression of the phase advance (caused by masking) and altered entrainment. Beyond the baseline, the differences observed between WT and mutant in the ZT 14 and ZT 22 light pulses together with the skeleton photoperiod results strongly support that there is an alteration in light responsiveness and entrainment for mutant mice. Interestingly, *Drosophila Tim2* knockdown affects the phase response to light (30). Furthermore, transient disruption of m*Tim* RNA across circadian time alters the phasing of circadian rhythmicity (17). TIM protein is predominantly and robustly expressed in proliferative organs compared with more differentiated tissues (18). We found that the period of mature peripheral tissues (lung and liver) from *RX*/+ mice was not altered, whereas the period of proliferating MEFs derived from *RX*/+ mice was moderately yet significantly shorter than that of +/+ mice (*SI Appendix*, Fig. S2*A*). Importantly, CRISPR generated *TIM R1081X*/+ heterozygous U2OS cells have a shortened period compared with +/+ control cells (Fig. 2*F*). Moreover, the period observed in HEK293 cells overexpressing *TIM R1081X* (*SI Appendix*, Fig. S2*C*) also showed shortening similar to that observed in CRISPR U2OS cells. Further studies are needed to unravel this discrepancy in period between mature vs. proliferating tissues and how this relates to behavioral phase advance in the setting of normal period in vivo.

Consistent with previously reported FASP mutations, *TIM R1081X* affects its stability and overall repressor activity inside the cell. With the exception of *PER2 S662G*, all of the FASP mutations render weakened repression of CLOCK/BMAL1-mediated transactivation and instability of the respective pro-

teins. The TIM R1081X protein localizes predominantly in the cytosol unlike TIM WT, which localizes to the nucleus (Fig. 4 *C* and *D*). NLS4-deleted TIM protein recapitulates the shortened period and altered subcellular localization phenotypes. The latter finding confirms the previously reported necessary role of C-terminal portion of mammalian TIM in its nuclear localization (18). Combining these results, we cannot say whether the TIM R1081X protein has reduced repressor activity itself, or whether its instability and extranuclear localization contribute to observed derepression of CLOCK/BMAL1-mediated transactivation. Nevertheless, the *TIM R1081X* mutation causes protein instability and overall reduced repression of BMAL1/CLOCK, which is consistent with other examples of FASP.

The protein levels of core clock components are known to play critical roles in maintaining clock stability. We show here that TIM R1081X can destabilize CRY1/2 and PER1/2. The association between TIM R1081X and CRY2 is weakened compared with TIM WT. PER2 also binds TIM, but the R1081X mutation does not alter this association. Interestingly, CRY1 and CRY2 have been reported to have opposing roles in the maintenance of period length (31, 32). Thus, the finding that TIM R1081X destabilizes both CRY1 and CRY2 may explain the lack of period change in mutant mice. Because the destabilization of CRY2 has been associated with phase behavior differences (7), this instability may continue to exert its effect in the context of phase alone and supports the idea that regulation of phase (phase advance of behavior) can be independent of period length. While the R1081X mutation destabilizes both PERs and CRYs, TIM WT does not increase PERs or CRYs stability when expressed alone. TIM WT destabilizes CRY2 and PER2 when they are both present, and this destabilization is further
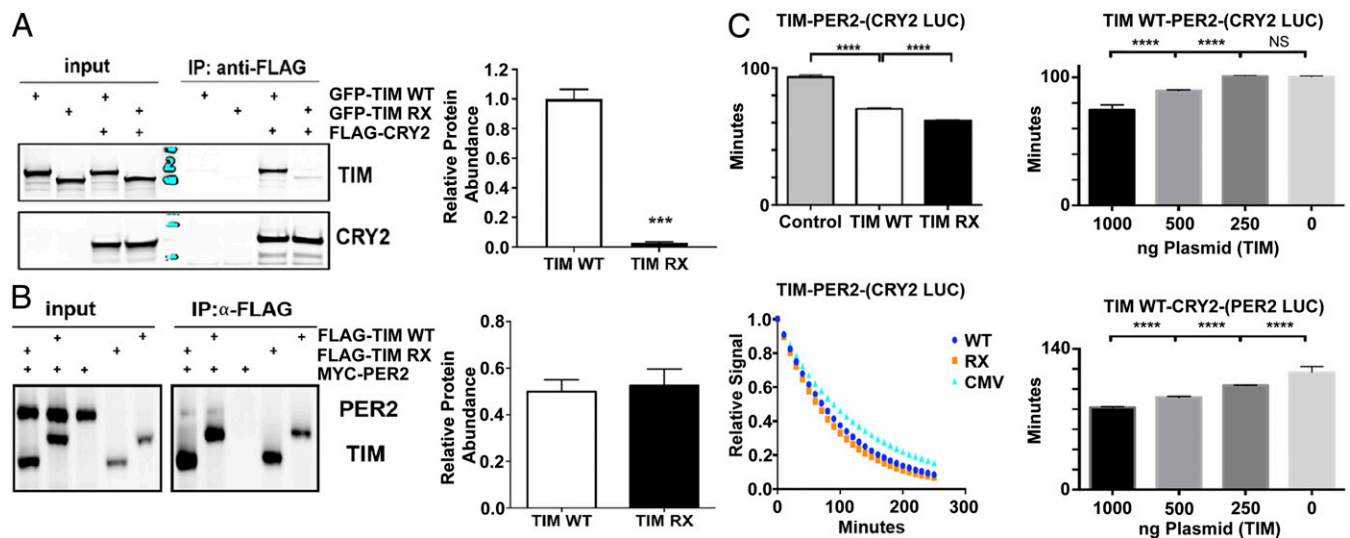
Fig. 5. TIM modulates PER2–CRY2 complex stability, and this modulation is altered by the R1081X mutation. (*A*) Coimmunoprecipitation of TIM WT or TIM R1081X by CRY2 in 293T lysates. CRY2-bound TIM was normalized to amount of bound TIM WT. Results are expressed as mean ± SEM (*n* = 5). ***$P < 0.001$ (Student's *t* test). (*B*) Coimmunoprecipitation of PER2 by TIM WT and TIM R1081X in 293T lysates. TIM-bound PER2 was normalized to the amount of input PER2. Results are expressed as mean ± SEM (*n* = 6); $P > 0.05$ (Student's *t* test). (*C*) *Left Upper* and *Left Lower* views show half-life and decay plots of CRY2:luc after HEK 293T cells were transfected with TIM WT, TIM R1081X, or CMV (vector control) and PER2 followed by CHX administration. *Right Upper* and *Lower* panels show a dose-dependent reduction in CRY2:luc (*Upper*) or PER2:luc (*Lower*) stability when cotransfected with increasing amounts of TIM WT. Results are expressed as mean ± SEM (*n* = 10). ****$P < 0.0001$; NS, not significant (one-way ANOVA with Tukey's multiple-comparisons test).

enhanced by the *R1081X* mutation. These results suggest the existence of a TIM–PER2–CRY2 complex in which TIM plays the role in fine-tuning the levels of CRY2/PER2. Collectively, these data demonstrate a role for mammalian *Timeless* in circadian regulation, and we posit that it has a role in destabilizing the PER–CRY complex in the cytoplasm, creating the conditional ability to adjust to minor changes in phase. How TIM nuclear migration is regulated may provide insight into its function as a destabilizer of PER and/or CRY proteins, and investigation into the precise functions of TIMELESS can further reveal the mechanism of phase modulation.

Materials and Methods

Nomenclature. For humans, the gene is *TIM*, and the protein is TIM. For mouse, the gene is *Tim*, and the protein is TIM. +/+ refers to WT animals or unaffected human subjects, and RX/+ refers to heterozygous mutant animals or affected human subjects, and similar terminology is used for CRISPR-modified cell lines.

Human Data and Mutation Screening. All human subjects signed a consent form approved by the Institutional Review Boards (IRBs) at the University of Utah and the University of California, San Francisco. All experiments involving human subjects were approved by the IRB Molecular Characterization of Circadian Rhythm Traits (IRB no. 10-03952). The consent form includes all confidentiality and ethics guidelines.

Subjects were characterized by a previously published procedure (22). The data were interpreted by one of the authors (either C.R.J. or L.J.P.) and characterized as possible, probable, or definite ASP (an earlier spontaneous awakening in the setting of an earlier sleep time) or as unaffected with consideration for confounding and masking influences, by the age of 30 (7). Subjects characterized as "definite ASP" had Horne–Ostberg questionnaire (H-O) scores of at least 70. Sleep logs, actigraphy, and Zeo (Zeo, Inc.) EEG recordings were obtained to characterize consecutive nights of sleep at home. Activity onset and offset were defined by actigraphy and sleep onset and offset were defined by Zeo recordings.

DNA was extracted from blood samples taken from members of kindred 5602, purified, and used to screen for mutations. Specific primers covering the coding sequence of the circadian candidate genes were used to amplify fragments for sequencing. The candidate genes screened included *CLOCK, BMAL1, PER1-3, CRY1-2, DEC1-2, CSNK1D, CSNK1E, PRKAA2, NPAS2, CSNK2A2, CSNK2B, FBXL3, GSK3B, PKCA, PRKAA1, PRKAA2, RAB3A, RORA, TIMELESS,*

NR1D1, and *PRKCG* as previously described (7). *TIMELESS R1081X* was identified as a genetic variant specific to this family, and it is not found in any public genome database as of June 2018.

Exome sequencing was performed on two individuals, one ASP and one control. Omicia Opal 0.10.0 software was used to annotate the variants for potential disease-causing mutations in the exomes of each of the affected individuals (after filtering out common variants, dbSNP minor allele frequency > 1%) using the HGMD and OMIM databases. Variant prioritization (using Ingenuity Variant Analysis) included generating a list of all variants, filtered for (*i*) minor allele frequency of <0.01% according to 1000 Genomes Project, Complete Genomics public genomes, and National Heart, Lung, and Blood Institute Exome Sequencing Project exomes; (*ii*) nonsynonymous, near a splice site/promoter, or a structural variant; and (*iii*) occur in affected and not in the control sample.

Wheel-Running and Circadian Analysis. *RX*/+ and +/+ mice were maintained on a C57BL/6J background. Experimental mice were male and ~8 wk old at the initiation of behavioral assays. Mice were individually housed in wheel-running cages with ad libitum access to food and water. Mice were initially entrained to LD 12:12 at 250 lux for at least 14 d. Onset times, offset times, and acrophase were analyzed using data from stably entrained mice to generate activity profiles using ClockLab software (Actimetrics; RRID SCR_014309). After entraining mice for a minimum of 14 d, mice were released into constant darkness (DD) to assess free-running period. Period determination was made with line fitting of activity onsets from day 1 to day 14 in DD using ClockLab software. To examine whether masking confounded observed locomotor behavior in LD conditions, a skeleton photoperiod was employed with two entrainment light pulses of 250 lux from clock times 6:00 to 6:15 to designate the "morning" light cue and again from clock times 17:45 to 18:00 to designate the "evening" light cue. Mice were kept on this schedule for 10 d after stable entrainment to LD 12:12 conditions. To determine phase-shifting behavior, mice were stably entrained to LD 12:12 conditions and then subjected to a 30-min light pulse (250 lux) from ZT 14 to ZT 14:30 or, separately from ZT 22 to ZT 22:30, and then the mice were released into DD for at least 10 d. Phase shifts were determined by line fitting of activity onsets from day 1 to day 10 in DD and compared with line fitting of activity onsets at baseline in DD conditions without a light pulse. All data collection and analysis were done using ClockLab software (Actimetrics; RRID SCR_014309). Activity onset and offset were defined using the ClockLab software algorithm.

EEG and Sleep–Wake Analysis. For EEG analysis, mice were surgically fitted with EEG electrodes. The mice were anesthetized using isoflurane anesthesia

and placed on the surgical stage, and the skull was immobilized. The hair was shaved, and betadine was applied to the scalp and allowed to dry. A vertical incision was made, and the skull was exposed with a sterile cotton swab. A 23-gauge sterile surgical needle was used to make four epidural guide holes through the skull over the frontal cortical area and over the parietal area (1 mm anterior to bregma, 1 mm lateral to the midline, and 3 mm posterior to bregma, 2.5 mm lateral to midline, respectively). One ground and three lead screws were surgically placed into the skull through the guide holes. The three lead screws were soldered onto a six-pin connector EEG/EMG head stage (Pinnacle Technologies). EMG leads from the head stage were surgically placed into the neck muscle and the base of the head stage was covered with black dental cement to form a solid cap on the head. The incision was closed with VetBond (3M; Santa Cruz Biotechnology), and animals were given a s.c. injection of Marcaine (0.05 mg/kg) adjacent to the vertical incisions before recovery on a heating pad. Mice were allowed to recover for 3 wk before behavioral analysis. During EEG/EMG recording, mice were singly housed, and a tethered preamplifier (to record EEG signals) was attached to the head stage. The mice habituated to the recording cable for 7 d in LD 12:12 conditions, allowing for freedom of movement in the base of the cage. EEG data were then collected in LD 12:12 conditions. Data were acquired with Sirenia software (Pinnacle Technologies). EEG signals were sampled at 500 Hz. A 24-h epoch of EEG data was prescored semi-automatically by Sirenia Sleep Pro software, and then subsequently hand-scored by researchers blinded to genotype.

Cell Culture and Constructs. HEK293 cells (ATCC CRL-3216; RRID: CVCL_0063) were purchased from ATTC. Authentication of the cell lines was performed using STR profiling by ATCC. A stable U2OS-B6 cell line that expresses a destabilized firefly luciferase gene under the control of the m*Bmal1* promoter was obtained from Satchidananda Panda, Regulatory Biology Laboratory, Salk Institute for Biological Studies, La Jolla, CA (33). All cell lines were confirmed as *Mycoplasma*-free every 6 mo. Cells were cultured in DMEM (Millipore Sigma) containing 10% FBS and maintained by standard methods. DNA constructs were introduced into the cells by using X-tremeGene 9 DNA Transfection Reagent (Roche). DNA constructs used were as follows: pCMV4a-CRY2-FLAG, pCMV2a-HA-CRY2, pCMV10-3xFLAG-CRY2, pCMV-GFP-TIM, pCMV-GFP-TIM R1081X, pCMV4a-TIM-FLAG, pCMV4a-TIM R1081X-FLAG, pCMV10-3xFLAG-TIM, pCMV10-3xFLAG-TIM R1081X, pCMV10-3xFLAG- hCRY2-WT-LUC, pCMV10-3xFLAG-hCRY1-WT-LUC, pCMV10-3xFLAG-hPER2-WT-LUC, pCMV10-3xFLAG-hPER1-WT-LUC, pCS2-MT-hPER2-WT, pCMV10-3xFLAG-TIM ΔNLS3 (R940_K950del), pCMV10-3xFLAG-TIM ΔNLS4 (N1184_R1199del), pSQT1313-TIM G1, pSQT1313-TIM G2, pSQT1313-TIM G5, pSQT1313-TIM G6, pSQT1601 (Addgene; no. 53369), pX458-TIM G1, pX458-TIM G5. For guide sequence, see *SI Appendix*, Table S1. For protein stability assays, CHX (100 μg/mL; Santa Cruz Biotechnology) was added to the culture for intended length of treatment (0–8 h). All cells were harvested 40-h posttransfection, and lysates were assayed by Western blots.

Western Blot Assays. For whole-cell extracts, HEK293 cells were lysed in Nonidet P-40 buffer (150 mM NaCl, 1.0% Nonidet P-40, 50 mM Tris, pH 8.0) plus complete Mini protease inhibitor mixture (Roche). Preparation of the cytosolic and the enriched nuclear fractions was prepared with the Nuclear Extract Kit (Active Motif). Immunoprecipitation was performed with Ezview Red Anti-FLAG M2 affinity gels (Millipore Sigma). Proteins were separated by SDS/PAGE and transferred to Immobilon-FL PVDF membranes (Millipore Sigma), which were then blocked by SuperBlock (PBS) Blocking Solution (Thermo Fisher Scientific). Primary antibodies were diluted in PBST buffer (8 mM Na$_2$HPO$_4$, 150 mM NaCl, 2 mM KH$_2$PO$_4$, 3 mM KCl, 0.05% Tween 20, pH 7.4) and interacted with blots at 4 °C overnight. The blots were then probed with IRDye secondary donkey anti-rabbit/mouse/goat antibodies (LI-COR) at room temperature for 1 h. The blots were imaged using the LI-COR Odyssey system (LI-COR). Protein intensities were measured using ImageJ software. β-Actin was used as a loading control. LaminB and GAPDH were used as nuclear and cytoplasmic markers, respectively. Relative protein levels or protein abundance were normalized to levels in the control group. Proteins were detected with the following antibodies: anti-HA (Abcam; ab9110), anti-FLAG M2 (Sigma-Aldrich; F1804), anti-GFP (Abcam; ab290), anti–β-actin (Abcam; AC-15), anti-GAPDH (Millipore Sigma; MAB374), anti-LaminB1 (Abcam, ab16048; Santa Cruz, C20), anti-mPER2 (Alpha Diagnostic International; PER-21A), anti-hCRY2 (Santa Cruz; sc-130731), and anti-hTIM (Abcam; ab50943).

Luciferase Assay. Dual-Luciferase Reporter Assay (Promega) was performed in HEK293T cells transfected with a *Per2::luc* reporter and other expression constructs 24 h posttransfection. For transfection, 100 ng per construct per well of a 24-well plate was used, except for TIM titration, when 100, 20, or 4 ng of *TIM-WT* or *TIM-R1081X* constructs were transfected. A constitutively expressed *Renilla* Luciferase construct was used as an endogenous control.

Luciferase activity was measured by Synergy H4 Hybrid Microplate Reader (BioTek). Results are expressed as mean ± SEM. All experiments were performed at least two times, and all data presented are the average of three technical replicates.

Immunocytochemistry. 293T cells were plated on two-well chamber slides (Nunc Lab-Tek II) and transfected with TIM expression constructs. Cells were then fixed, permeabilized, and exposed to primary and secondary antibodies. Images were taken under a fluorescence microscope (Olympus). The LSM images were projected and quantified using ImageJ. Cell nucleus boundary was defined by DAPI-stained area. TIM immunocytochemical signal from cell body and nucleus of individual cells was calculated as total integrated density minus background of the cell body area.

Generation of *Tim-R1078X* Mice. Single guide RNAs (sgRNAs) were generated by MEGAshortscript T7 Transcription Kit (Thermo Fisher Scientific) and quantitated by NanoDrop (Thermo Fisher Scientific), according to Ran et al. (34). One-cell stage C57BL/6 embryos were injected with Cas9 mRNA, sgRNAs, and 200-nt single-stranded oligodeoxynucleotides (ssODN) (purchased from IDT) repair template and later transplanted to surrogate mothers. Fifteen animals were born and genotyped by TaqMan genotyping to identify founders (*SI Appendix*, Fig. S1B). The *Tim R1078X* allele was verified by Sanger sequencing in founder #1L. The founder was backcrossed once to generate N1 mice. N1 littermates were then crossed to expand the colony. Sequences of guide, ssODN repair template, primer, and probe are listed in *SI Appendix*, Table S1. All mouse work was performed in accordance with the guidelines of Institutional Animal Care and Use Committee at the University of California, San Francisco.

Generation of *TIM-R1081X* U2OS Cell Line. Guide RNAs were picked using MIT CRISPR Design (http://zlab.bio/guide-design-resources) and cloned into pX458 plasmids (Addgene; no. 62988), according to Ran et al. (34). Cells were cultured for 24 h before guide plasmid and 200-nt ssODN repair template (IDT) were delivered by nucleofection (Nucleofector 2b; Lonza). After 36–48 h, GFP-positive single-cell clones were isolated in 96-well plates (34). Surviving and expanded clones were genotyped by TaqMan genotyping to identify founders (Fig. 2D). The *TIM-R1081X* allele was verified by Sanger sequencing in U2OS clone 37 (Fig. 2E). Guide, primer, and probe sequences are listed in *SI Appendix*, Table S1.

Bioluminescence Rhythms in Tissue Culture. *Tim-RX* mutant mice were crossed with m*Per2^{Luc}* knockin mice (23) (RRID IMSR_ JAX006852). Mice were killed between ZT2 and ZT3. Liver and lung were harvested. Liver tissues were thinly sliced under sterile conditions and cultured on Millicell culture membrane (PICMORG50; EMD Millipore) in 35-mm dishes with 1.4 mL of recording medium [phenol-red free DMEM (Sigma-Aldrich) containing 10 mM Hepes (pH 7.0), 3.5 g/L D-glucose, 0.2 mM luciferin potassium salt, 0.35 g/L sodium bicarbonate, 2% B-27 supplement (Thermo Fisher Scientific), 50 U/mL penicillin–streptomycin (Thermo Fisher Scientific)]. Lung tissues were removed in small cubes and placed directly on 35-mm dishes which were allowed to adhere for 10 min before the addition of recording medium. Bioluminescence was recorded continuously in a LumiCycle 32 instrument (Actimetrics). Bioluminescence was detrended by subtracting 24-h average of bioluminescence using the LumiCycle analysis software. The period length of each sample was determined by dampened sine-curve fitting using LumiCycle analysis.

Luciferase-Based Degradation Assay. HEK293T cells were cotransfected using Lipofectamine 3000 (Thermo Fisher Scientific) with 50 ng hCRY2/1-LUC or hPER2/1-LUC vectors and 1,000, 500, or 200 ng, TIM-WT, or TIM-RX, and/or PER2-WT or CRY2 WT, or empty CMV-10 vectors and cultured for 24 h. The culture medium was replaced with recording medium [phenol-red free DMEM (Sigma Aldrich) supplemented with 10% FBS, 3.5 mg/mL glucose, 50 U/mL penicillin-streptomycin (Thermo Fisher Scientific), 0.05 mM luciferin, and 10 mM Hepes-NaOH; pH 7.0] containing 100 mg/mL CHX (Santa Cruz Biotechnology). Luciferase activity of hCRY2-LUC of hPER2-LUC was recorded at 10-min intervals at 37 °C with a LumiCycle 32 instrument (Actimetrics). The luminescence signals were fitted to an exponential function to quantify the half-life of CRY2-LUC or PER2-LUC.

1. D. P. King, J. S. Takahashi, Molecular genetics of circadian rhythms in mammals. *Annu. Rev. Neurosci.* **23**, 713–742 (2000).
2. J. A. Mohawk, C. B. Green, J. S. Takahashi, Central and peripheral circadian clocks in mammals. *Annu. Rev. Neurosci.* **35**, 445–462 (2012).
3. J. S. Takahashi, Transcriptional architecture of the mammalian circadian clock. *Nat. Rev. Genet.* **18**, 164–179 (2017).
4. S. M. Reppert, D. R. Weaver, Molecular analysis of mammalian circadian rhythms. *Annu. Rev. Physiol.* **63**, 647–676 (2001).
5. P. L. Lowrey, J. S. Takahashi, Mammalian circadian biology: Elucidating genome-wide levels of temporal organization. *Annu. Rev. Genomics Hum. Genet.* **5**, 407–441 (2004).
6. K. L. Toh et al., An hPer2 phosphorylation site mutation in familial advanced sleep phase syndrome. *Science* **291**, 1040–1043 (2001).
7. A. Hirano et al., A Cryptochrome 2 mutation yields advanced sleep phase in humans. *eLife* **5**, e16695 (2016).
8. Y. Xu et al., Modeling of a human circadian mutation yields insights into clock regulation by PER2. *Cell* **128**, 59–70 (2007).
9. Y. Xu et al., Functional consequences of a CKIdelta mutation causing familial advanced sleep phase syndrome. *Nature* **434**, 640–644 (2005).
10. P. Jiang, K. M. Franklin, M. J. Duncan, B. F. O'Hara, J. P. Wisor, Distinct phase relationships between suprachiasmatic molecular rhythms, cerebral cortex molecular rhythms, and behavioral rhythms in early runner (CAST/EiJ) and nocturnal (C57BL/6J) mice. *Sleep (Basel)* **35**, 1385–1394 (2012).
11. P. Vinayak et al., Exquisite light sensitivity of *Drosophila melanogaster* cryptochrome. *PLoS Genet.* **9**, e1003615 (2013).
12. Z. Yang, M. Emerson, H. S. Su, A. Sehgal, Response of the timeless protein to light correlates with behavioral entrainment and suggests a nonvisual pathway for circadian photoreception. *Neuron* **21**, 215–223 (1998).
13. M. Rosbash et al., A *Drosophila* circadian clock. *Cold Spring Harb. Symp. Quant. Biol.* **61**, 265–278 (1996).
14. C. Benna et al., A second *timeless* gene in *Drosophila* shares greater sequence similarity with mammalian *tim*. *Curr. Biol.* **10**, R512–R513 (2000).
15. A. L. Gotter et al., A time-less function for mouse *Timeless*. *Nat. Neurosci.* **3**, 755–756 (2000).
16. S. A. Tischkau et al., Oscillation and light induction of *timeless* mRNA in the mammalian circadian clock. *J. Neurosci.* **19**, RC15 (1999).
17. J. W. Barnes et al., Requirement of mammalian *Timeless* for circadian rhythmicity. *Science* **302**, 439–442 (2003).
18. E. Engelen et al., Mammalian TIMELESS is involved in period determination and DNA damage-dependent phase advancing of the circadian clock. *PLoS One* **8**, e56623 (2013).
19. N. Koike et al., Identification of the mammalian homologues of the *Drosophila* timeless gene, *Timeless1*. *FEBS Lett.* **441**, 427–431 (1998).
20. A. M. Sangoram et al., Mammalian circadian autoregulatory loop: A *timeless* ortholog and *mPer1* interact and negatively regulate CLOCK-BMAL1-induced transcription. *Neuron* **21**, 1101–1113 (1998).
21. M. J. Zylka et al., Molecular analysis of mammalian *timeless*. *Neuron* **21**, 1115–1122 (1998).
22. C. R. Jones et al., Familial advanced sleep-phase syndrome: A short-period circadian rhythm variant in humans. *Nat. Med.* **5**, 1062–1065 (1999).
23. S.-H. Yoo et al., PERIOD2:LUCIFERASE real-time reporting of circadian dynamics reveals persistent circadian oscillations in mouse peripheral tissues. *Proc. Natl. Acad. Sci. U.S.A.* **101**, 5339–5346 (2004).
24. C. Jud, I. Schmutz, G. Hampp, H. Oster, U. Albrecht, A guideline for analyzing circadian wheel-running behavior in rodents under different lighting conditions. *Biol. Proced. Online* **7**, 101–116 (2005).
25. R. Dallmann, J. P. DeBruyne, D. R. Weaver, Photic resetting and entrainment in CLOCK-deficient mice. *J. Biol. Rhythms* **26**, 390–401 (2011).
26. K. Vanselow et al., Differential effects of PER2 phosphorylation: Molecular basis for the human familial advanced sleep phase syndrome (FASPS). *Genes Dev.* **20**, 2660–2672 (2006).
27. L. Zhang et al., A *PERIOD3* variant causes a circadian phenotype and is associated with a seasonal mood trait. *Proc. Natl. Acad. Sci. U.S.A.* **113**, E1536–E1544 (2016).
28. K. Unsal-Kaçmaz, T. E. Mullen, W. K. Kaufmann, A. Sancar, Coupling of human circadian and cell cycles by the timeless protein. *Mol. Cell Biol.* **25**, 3109–3116 (2005).
29. T. Takumi et al., A mammalian ortholog of *Drosophila timeless*, highly expressed in SCN and retina, forms a complex with mPER1. *Genes Cells* **4**, 67–75 (1999).
30. C. Benna et al., *Drosophila timeless2* is required for chromosome stability and circadian photoreception. *Curr. Biol.* **20**, 346–352 (2010).
31. M. H. Vitaterna et al., Differential regulation of mammalian period genes and circadian rhythmicity by cryptochromes 1 and 2. *Proc. Natl. Acad. Sci. U.S.A.* **96**, 12114–12119 (1999).
32. G. T. J. van der Horst et al., Mammalian Cry1 and Cry2 are essential for maintenance of circadian rhythms. *Nature* **398**, 627–630 (1999).
33. C. Vollmers, S. Panda, L. DiTacchio, A high-throughput assay for siRNA-based circadian screens in human U2OS cells. *PLoS One* **3**, e3457 (2008).
34. F. A. Ran et al., Genome engineering using the CRISPR-Cas9 system. *Nat. Protoc.* **8**, 2281–2308 (2013).

NEUROSCIENCE